Particle-scale interaction in sand-rubber mixtures and their influence on energy dissipation mechanisms

Fonseca, J. [1*], Riaz, A. [1] Bernal-Sanchez, J.[2], Barreto, D. [2], McDougall, J. [2], Miranda-Manzanares, M. [3], Marinelli, A. [2] and Dimitriadi, V. [2]

*Corresponding Author

Joana.Fonseca.1@city.ac.uk

ABSTRACT

Sand-rubber mixture (SRm) behaviour is affected by rubber content (RC) whilst dissipation in sands is caused by inter-particle sliding. Dissipation in SRm is as, or more significant than in sands. However, the mechanisms of dissipation in SRm are not well understood. In this study, one-dimensional compression tests on sand samples with RC of 0%, 15%, 30%, 45% and 100% by mass were performed on a standard oedometer. In addition, a SRm with RC of 30% was tested on a mini-oedometer placed inside an X-ray scanner and 3D images of the internal structure of the material were acquired at three stages during loading and unloading. Image analysis was used to infer particle-scale measurements and provide experimental evidence to help explaining the energy dissipation mechanisms for SRm. It is postulated here that energy dissipation in these mixtures is dominated by inter-particle sliding at initial stages of loading, but once rubber particles fill the voids spaces between the sand, deformation and dissipation mechanisms are dominated by the deformation of the rubber particles.

KEYWORDS

Fabric/structure of soils; Particle-scale behaviour; Sand–rubber mixtures; Compressibility; Microscopy; Laboratory tests

---

[1] City, University of London, London, UK

[2] Edinburgh Napier University, UK

[3] University of Cantabria, Spain

INTRODUCTION

Previous research on the behaviour of sand-rubber mixtures (SRm) has demonstrated that using tyre shreds can lead to shear strength increases (e.g. Edil & Bosscher, 1994; Foose et al., 1996; Zornberg et al., 2004; Mashiri et al., 2015a; Mashiri et al., 2015b; Fu et al., 2014; Fu et al., 2017). On the other hand, when rubber crumbs were used a decrease in shear strength was observed (e.g. Masad et al., 1996; Youwai & Bergado, 2003; Sheikh et al., 2012). An increase in the rubber content is believed to be associated to a reduction in the stiffness of the material (e.g. Zheng-Yi & Sutter, 2000; Anastasiadis et al., 2012; Senetakis et al., 2012; Nakhaei et al., 2012; Ehsani et al., 2015; Pistolas et al., 2018). In fact, variations in rubber content can result in rubber-like or sand-like behaviours (Lee et al. 2007; Lee et al., 2014; Kim & Santamarina, 2008; Senetakis & Anastasiadis, 2015).

Existing evidence considers the dynamic behaviour of SRm under less than 10 loading-unloading cycles. The consensus is that energy dissipation in SRm is as, or more significant than in sands (e.g. Zheng-Yi & Sutter 2000; Senetakis et al., 2012; Ehsani et al., 2015).

In summary, geotechnical properties of SRm are affected by rubber content, particle size, particle shape, and size ratio between compressible and rigid particles, amongst other factors. However, experimental evidence at the particle scale is very limited. This study aims to gain further understanding on the particle-scale mechanisms that underlie the observed energy dissipation mechanisms of RSm. The effect of rubber particle shape was qualitatively assessed by means of plane strain tests on mixtures of rubber particles and acrylic discs. On the other hand, the influence of rubber content is evaluated via standard oedometer tests on SRm. Finally, grain-scale measurements of a mini-oedometer sample carried out on a SRm with 30% RC are presented in order to quantify changes of contact area between sand and rubber particles under different loading regimes. This set of experiments is then discussed to provide further insight into the potential microscale mechanisms that underlie energy dissipation in SRm.

PLAIN STRAIN EXPERIMENTS

Plane strain models of acrylic discs mixed with rubber particles of different shapes and sizes were developed to preliminarily observe particle scale interaction mechanisms in SRm. In order to make qualitative observations on the effect of the rubber particle shape, two rubber particle aspect ratios were used in conjunction with acrylic discs of 6 mm diameter as shown in Figs. 1 and 2. Rubber crumbs (Fig. 1) had an aspect ratio (AR) between 1.0 and 1.5 while the size ratio (SR) between rubber and acrylic discs was approximately 1.0. Rubber shreds (Fig. 2) had an aspect ratio (AR) between 5 and 6 while the size ratio between shreds and acrylic discs varied between 2 and 3. The plane strain apparatus for the experiments shown in Figs. 1 and 2 consisted of an A4-size acrylic sheet with PVC

flat bars used as lateral boundaries. Two vertical flat bars of made PVC of 20 mm width and 2 mm thickness were fixed to the sides of the acrylic base using screws to provide lateral constraint. A similar PVC flat bar was fixed horizontally to the bottom in order to provide a fixed base to the particles. Loading in the vertical direction was carried out by moving an additional "top" PVC bar attached to a sliding slot along the lateral (fixed) boundaries that enabled accurate control of the specimen's vertical dimension and provided a constant normal stress. Due to the geometry of the rubber and acrylic particles any deformations in the out of plane direction are prevented and plane strain conditions are guaranteed. Fig. 1 shows a mix of mono-disperse acrylic discs mixed with rubber crumbs before (Fig. 1a) and after compression (Fig. 1b) under a nominal one-dimensional load and lateral deformation constraint. It can be seen that during loading the area of contact of rubber particles with acrylic and other rubber particles increases. This is evidenced by changes in the shape of the rubber crumbs at the boundary between rubber particles and acrylic discs.

Fig. 2 shows the effect of loading on the behaviour of an assembly of acrylic discs and shredded rubber particles. The material, sample preparation and loading are equal to those used for crumbs. Hence, differences are due to rubber particle only. By comparing Fig. 2a and Fig. 1a observations on the initial density can be made. The specimen with rubber shreds has a higher void ratio than that made with rubber crumbs. Fig. 2b shows that during loading the rubber shreds have deformed and by wrapping around the acrylic discs the contact area between rubber and acrylic has increased with respect to the conditions in Fig 2a. Note that not all rubber shreds deform in equal manner. The increased contact area is not homogeneous and/or proportionally equivalent across all rubber shreds. This indicates the existence of a non-homogeneous stress transmission between particles (i.e. force chains). Furthermore, by comparing Fig. 1b and Fig. 2b we can state that the mechanisms of stress transmission at inter-particle contacts in rubber shreds are significantly different to those observed in rubber crumbs. The qualitative changes observed are more significant in rubber shreds than in rubber crumbs. This justifies the detailed experimental investigation using SRm with rubber shreds that follows.

MACROSCALE BEHAVIOUR OF SRm FROM OEDOMETER TESTS

A series 100 mm diameter oedometer tests using (air pluviated) sand-rubber mixtures with shredded rubber particles were performed. Sub-angular Leighton Buzzard sand particles (LBS) with a mean particle diameter of 0.85 mm were mixed with recycled devulcanised shredded rubber particles at rubber contents of 0%, 15%, 30% and 45% by mass. Shredded rubber particles with particle diameter similar to that of the sand were used. The length of the shredded particles varied between 1 mm and 6 mm.

Fig. 3 shows the one-dimensional (oedometric) behaviour of the SRm. The response of the sand-only sample is unsurprisingly stiffer than that of any SRm, and even at large stress levels the amount of vertical deformation is limited and the stress-strain response is nearly linear. We refer to this as "sand-like" response. In contrast, for RC of 100% the vertical strain is significant, dependent on stress level and the stress-strain response in addition to being significantly non-linear, shows clear evidence of plastic deformation. We refer to this behaviour as "rubber-like" response. These patterns of behaviour have also been observed in previous studies (e.g. Lee et al., 2010; Kim & Santamarina, 2008). Traditionally, the magnitude of energy dissipation is calculated by estimating the area of an hysteresis loop in the shear stress vs shear strain space. In order to do this with the data presented in Fig. 3 an assumption regarding the value of the coefficient of earth pressure at rest (K_0) would be required. Nevertheless, the area between each loading-unloading loop in Fig. 3 is a measure of energy dissipation, but comments can only be made in relation to the nature of energy dissipation (i.e. shape of the loading/unloading loops in Fig. 3). Fig. 3 demonstrates that energy dissipation is dependent on rubber content and stress level. As a matter of interest, the dissipation of energy in all samples is higher during the first loading-unloading cycle. This is confirmed by a larger accumulation of plastic deformation during the first cycle in comparison with subsequent cycles. This suggests that the mechanisms involved in energy dissipation are also dependent on the void ratio.

With reference to Fig. 3 and as discussed before, all specimens exhibit a larger magnitude of dissipation during the first loading/unloading cycle (as evidenced by a larger accumulation of plastic deformation). This phase can be explained for both sand only and SRm specimens in terms of particle re-arrangement and sliding at interparticle contacts (Zheng-Yi & Sutter, 2000; Anatasiadis et al., 2012). On the other hand the linearity of the sand-like response is explained by the inability of sand grains to slide back to their original position during unloading. Changes in void ratio are limited in subsequent loading/unloading cycles. In contrast, the non-linearity and dependence of the rubber-like response on stress level and rubber contact can be explained by the deformability of the compressible particles. During the first loading/unloading cycle dissipation is likely to occur due to particle sliding. However, in subsequent cycles as the stress level increases the compressible particles deform more significantly. As this happens the volume of voids reduces (filled by deformed rubber particles) and the contact area increases between both rubber and sand particles. Rubber particles can then fulfil two different roles: one which participates in the loading transmission and the other which acts like a void inert portion (Platzer et al., 2018). Whilst the behaviour of rubber particles can be expected to be nearly elastic, the inter-particle friction in rubber is significantly high (e.g. Lopera Perez et al., 2016). As a result, as contact area increases with stress level, the high inter-particle friction does not enable dissipation to occur due to inter-particle sliding. Energy dissipation therefore can only be explained in terms of the changes of void ratio in the specimen during the loading/unloading cycles, which is in turn caused by the deformability of rubber particles and their void filling capacity during loading.

The microscale experiments described in the next section have been developed to provide experimental evidence that supports these postulates.

MICROSCALE QUANTIFICATION

In order to validate the hypotheses postulated above, a microscale investigation was carried out on a rubber-sand mixture (30% rubber by mass) composed of the same sand and shredded rubber particle types used in the previous oedometer tests. A mini-oedometer with an internal diameter of 14mm was operated inside an X-ray scanner in order to obtain images of the internal microstructure of the mixtures as they deform under loading and unloading. The X-ray scanner system used was a Nikon XTH 225 ST located at the Research Centre at Harwell, Oxfordshire (UK). The experimental set-up consisted of a load cell, a vertical piston, a micrometer and a small oedometer. The set-up was designed for this particular scanner and was mounted on the rotating table of the scanner, more details on the equipment can be found in Nadimi & Fonseca (2018). The size of the specimen was 14 mm in diameter and 11 mm high. The force was exerted by manually screwing the micrometer until the pre-set load was reached. A high precision micrometer with an axial loading capacity of 450 N was used. The sample container was made of Perspex with 2 mm thickness for which a value of less than 3 μm deflection under the maximum applied force was measured. The lateral friction has been minimized by allowing a 1 mm gap between the container and the X-ray window. The exerted force was monitored by a low profile 'pancake type' load cell with a 500 N capacity.

The images were acquired at three stages: prior to loading (Stage 0), under a vertical load of 120N (Stage 1) and after unloading to 35N (Stage 2). A total of 3142 projections were collected per scan, with an exposure of 500 ms per projection. The 3D images acquired had a resolution of 9.2 μm (length of voxel edge). In an X-ray scanning, the objects within the sample attenuate different levels of X-ray beam energy, depending on the material composition and density. Denser materials, the sand, attenuate more than less dense materials, the rubber and void space, and this difference in attenuation is represented by the intensity values of the voxels (volumetric pixels). The contrast of intensity level allows for differentiation of the three phases within the image, shown in Fig. 4. The rubber (darker grey) has intensity values between the void (black) and the sand grains (brighter grey).

An in-house imaging processing code was developed in Matlab (Mathworks, 2018) to segment the images by separating the three phases. This includes a two-step binarisation using Otsu's thresholding (Otsu, 1979), for which the sand phase was first isolated and secondly the rubber phase was separated from the void space. Horizontal and vertical sections through the 3D segmented images at the three stages of loading are presented in Fig. 5. The subsequent step of image processing was to identify the contacts between the sand grains and the rubber (Fonseca at al., 2013). The measurements consisted in counting the number of voxels forming each of the three phases and the contact regions. The volumes of sand, rubber and void space where obtained by multiplying the number of voxels by the

voxel size (9.2μm) ^{3}. For the contact areas the number of voxels was multiplied by (9.2μm)^2 to obtain the area of surfaces.

Table 1 shows the height of the sample, measured from the 3D images, at the three stages and the void ratio. The void ratio (e_{im}) was calculated as:

$$e_{im} = \frac{N_{voxel}^{void}}{N_{voxels}^{sand} + N_{voxels}^{rubber}} \quad (1)$$

where N_{voxel}^{void} is the number of voxels forming the void space within the sample, N_{voxels}^{sand} is the number of voxels occupied by sand grains and N_{voxels}^{rubber} is the number of voxels occupied by rubber.

The evolution of the rubber volume under loading and unloading is presented in Fig. 6 together with the evolution of the sample void ratio. It can be seen that the rubber undergoes volumetric compression when the loads increases to 120 N and on unloading to 35 N almost all the deformation is recoverable, as expected. The evolution of the contact area between the sand grains and the rubber is presented in Fig. 7. In this case, we can see an increase in the contact area as the applied load increases and on unloading only part of the newly formed contact areas are lost. This is an interesting finding and it appears to mimic (qualitatively) the evolution of the void ratio.

DISCUSSION AND CONCLUSIONS

Results obtained from a mini-oedometer inside an X-ray scanner have indicated that the contact area between sand and shredded rubber particles increases upon loading and only very slightly reduces during unloading. Similar observations were made in terms of void ratio. This occurs with very high inter-particle friction at contacts of rubber particles. Hence energy dissipation mechanisms at the macro-level are the result of physical phenomena at the micro-level. It has been shown that the common dissipation mechanism in sands (i.e. inter-particle sliding) only occurs during the initial loading-unloading cycle for SRm. After this point rubber particles "lock" and their deformation and void-filling capacity dominates the dissipation mechanisms. These mechanisms have been postulated based on quantitative image analysis, but also based on standard oedometers tests on SRm comprised of Leighton Buzzard sand and rubber shreds following preliminary analyses on plane strain models of acrylic discs and rubber particles of different shapes. The results across the three different experimental set-ups support the authors' hypotheses and provide an explanation of the micro-scale interactions affecting the observed macro-scale behaviour.

REFERENCES

Anastasiadis, A., Senetakis, K., Pitilakis, K., Gargala, C., Karakasi, I, Edil, T. & Dean, S.W. (2012). Dynamic Behavior of Sand/Rubber Mixtures. Part I: Effect of Rubber Content and Duration of

Confinement on Small-Strain Shear Modulus and Damping Ratio. *Journal of ASTM International* **9**, No. 2. DOI: 10.1520/JAI103680.

Edil, T.B. & Bosscher, P.J. (1994). Engineering Properties of Tire Chips and Soil Mixtures. *Geotechnical Testing Journal* **17**, No. 4, 453-464. DOI: 10.1520/GTJ10306J.

Ehsani,M, Shariatmadari, N. & Mirhosseini, S.M. (2015). Shear Modulus and Damping Ratio of Sand-Granulated Rubber Mixtures. *Journal of Central South University* **22** No.8, 3159–3167. DOI: 10.1007/s11771-015-2853-7.

Fonseca, J., O'Sullivan, C., Coop, M.R. & Lee, P.D. (2013). Quantifying the Evolution of Soil Fabric during Shearing using Scalar Parameters. *Géotechnique* **63**, No. 10, 818-829.

Foose, G.J., Benson, C.H. & Bosscher, P.J. (1996). Sand Reinforced with Shredded Waste Tires. *Journal of Geotechnical Engineering* **122**, No. 9, 760–767. DOI: 10.1061/(ASCE)0733-9410(1996)122:9(760).

Fu, R., Coop, M.R. & Li, X.Q. (2014). The Mechanics of a Compressive Sand Mixed with Tyre Rubber. *Géotechnique Letters* **4**, No. 3, 238–243.

Fu, R., Coop, M. & Li, X.Q. (2017). The Influence of Particle Type on the Mechanics of Sand-Rubber Mixtures. *Journal Geotechnical and Geoenvironmental Engineering* **143**, No. 9. DOI: 10.1061/(ASCE)GT.1943-5606.0001680.

Kim, H.K. & Santamarina, J.C. (2008). Sand–Rubber Mixtures (Large Rubber Chips). *Canadian Geotechnical Journal* **45**, No. 10, 1457–1466. DOI: 10.1139/T08-070.

Lee, C., Truong, Q. H., Lee, W. & Lee, J.S. (2010). Characteristics of Rubber-Sand Particle Mixtures According to Size Ratio. *Journal of Materials in Civil Engineering* **22**, No. 4, 323–331. DOI: 10.1061/(ASCE)MT.1943-5533.

Lee, C., Shin, H., & Lee, J.-S. (2014). Behavior of sand–rubber particle mixtures: Experimental observations and numerical simulations. *Int. J. Numer. Anal. Methods Geomech*., **38**, No. 16, 1651–1663.

Lee, J.S, Dodds, J. & Santamarina, J.C. (2007). Behavior of Rigid-Soft Particle Mixtures. *Journal of Materials in Civil Engineering* **19:2**, No. 179, 179–184. DOI: 10.1061/(ASCE)0899-1561(2007).

Lopera Perez, J.C., Kwok, C.Y. & Senetakis, K. (2016). Effect of Rubber Size on the Behaviour of Sand Rubber Mixtures: A Numerical Investigation. *Computers and Geotechnics* **80**, 199-214. DOI: 10.1016/j.compgeo.2016.07.005

Masad, E., Taha, R., Ho, C. & Papagiannakis, T. (1996). Engineering Properties of Tire/Soil Mixtures as a Lightweight Fill Material. *Geotechnical Testing Journal* **19**, No. 3, 297–304. DOI: 10.1520/GTJ10355J.

Mashiri, M.S., Vinod, J.S., Sheikh, M.N. & Tsang, H.H. (2015a). Shear Strength and Dilatancy Behaviour of Sand-Tire Chip Mixture. *Soils and Foundations Journal* **55**, No. 3, 517–528.

Mashiri, M.S., Vinod, J.S. & Sheikh, M.N. (2015b). Constitutive Model for Sand-Tyre Chip Mixtures. *International Journal in Geomechanics* **16**, No. 1.

Mathworks (2018) MATLAB release R2018a. Mathworks Inc, Natick

Nadimi, S. & Fonseca, J. (2018). Image based simulation of one-dimensional compression tests on carbonate sand. *Meccanica*. DOI: https://doi.org/10.1007/s11012-018-0923-2

Nakhaei, A., Marandi, S.M., Sani Kermani, S. & Bagheripour, M.H. (2012). Dynamic Properties of Granular Soils Mixed with Granulated Rubber. *Soil Dynamics and Earthquake Engineering* **43**, 124-132. DOI: 10.1016/j.soildyn.2012.07.026.

Otsu, N. (1979). A threshold selection method from gray-level histograms. *IEEE Trans. Sys., Man, Cyber* **9**, No. 1, 62–66.

Pistolas, G.A., Anastasiadis, A. & Pitilakis, K. (2018). Dynamic Behaviour of Granular Soil Materials Mixed with Granulated Rubber: Influence of Rubber Content and Mean Grain Size Ratio on Shear Modulus and Damping Ratio for a Wide Strain Range. *Innovative Infrastructure Solutions* **3**, No. 47. DOI: 10.1007/s41062-018-0156-1.

Platzer, A., Rouhanifar, S., Richard, P., Cazacliu, B. & Ibraim, E. (2018) Sand–Rubber Mixtures Undergoing Isotropic Loading: Derivation and Experimental Probing of a Physical Model. *Granular Matter* **20**, No. 4, 1–10. DOI: 10.1007/s10035-018-0853-7.

Senetakis, K., Anastasiadis, A. & Pitilakis, K. (2012). Dynamic Properties of Dry Sand/Rubber (SRM) and Gravel/Rubber (GRM) Mixtures in a Wide Range of Shearing Strain Amplitudes. *Soil Dynamics and Earthquake Engineering* **33**, No 1. 38-53. DOI: 10.1016/j.soildyn.2011.10.003.

Senetakis, K. & Anastasiadis, A. (2015). Effects of State of Test Sample, Specimen Geometry and Sample Preparation on Dynamic Properties of Rubber-Sand Mixtures. *Geosynthetics International Journal* **22**, No. 4, 301–310.

Sheikh, M.N., Mashiri, M.S., Vinod, J.S. & Tsang, H.H. (2012). Shear and Compressibility Behaviours of Sand-Tyre Crumb Mixtures. *Journal of Materials in Civil Engineering* **25**, No. 10, 1366-1374. DOI: 10.1061/(ASCE)MT.1943-5533.0000696.

Youwai, S. & Bergado, D.T. (2003). Strength and Deformation Characteristics of Shredded Rubber Tire – Sand Mixtures. *Canadian Geotechnical Journal* **40**, No. 2, 254–264. DOI: 10.1139/t02-104.

Zheng-Yi, F. & Sutter, K.G. (2000). Dynamic Properties of Granulated Rubber/Sand Mixtures. *Geotechnical Testing Journal* **23**, No. 3, 338–344.

Zornberg, J.G., Cabral, A.R., & Viratjandr, C. (2004). Behaviour of Tire Shred–Sand Mixtures. *Canadian Geotechnical Journal* **41**, No. 2, 227–241.

LIST OF FIGURES

LIST OF TABLES

NOTATION LIST

e_{im} void ratio measured from the 3D images

N_{voxel}^{void} number of voxels forming the void space within the sample

N_{voxels}^{sand} number of voxels occupied by sand grains

N_{voxels}^{rubber} number of voxels occupied by rubber

	Stage 0	Stage 1	Stage 2
Load (N)	0	120	35
Sample height (mm)	11.14	10.24	10.51
Void ratio (e_{im})	0.441	0.345	0.358

Figure 1a

Click here to access/download;Figure;Fig1a.tif

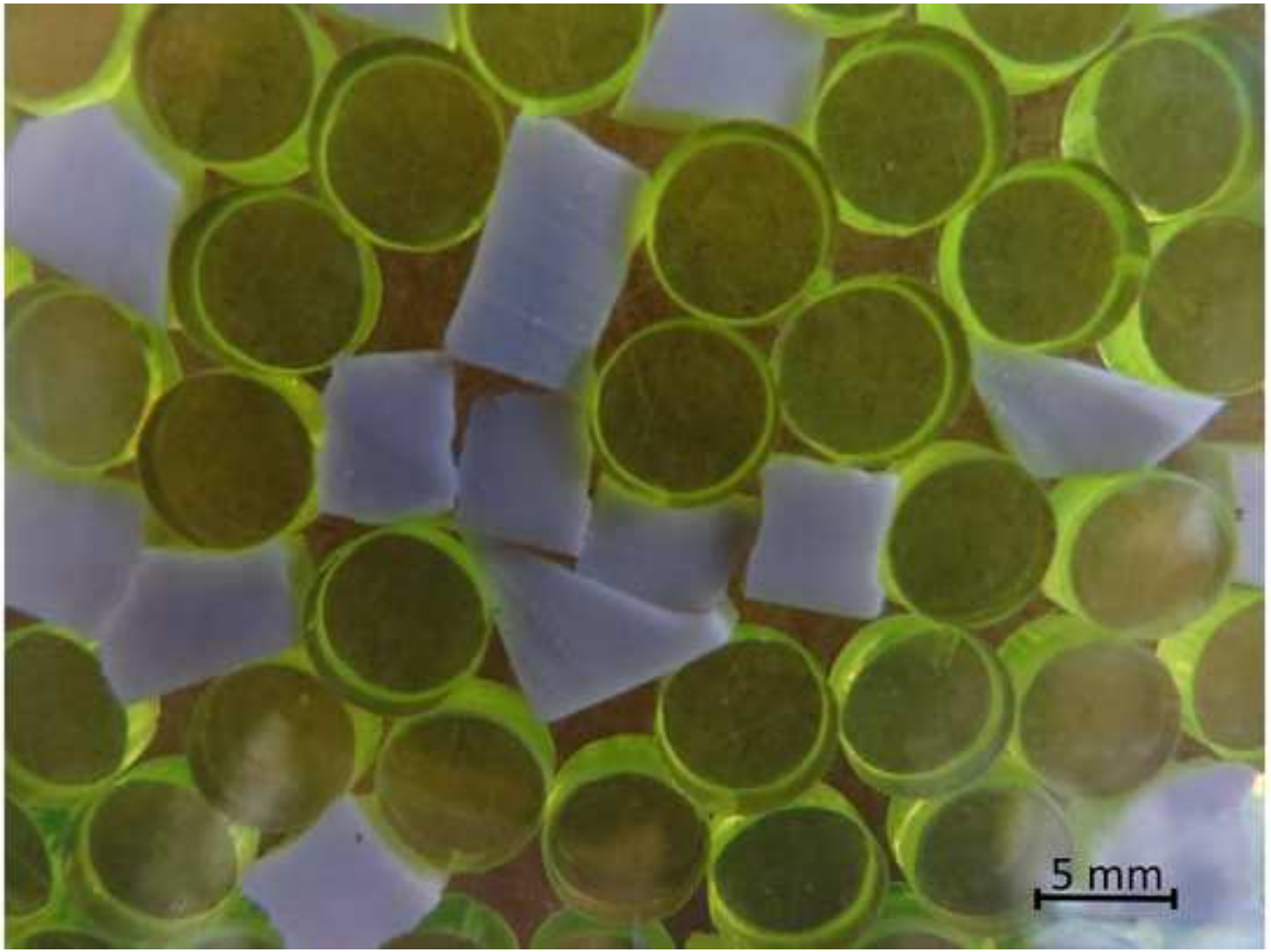

Figure 1b

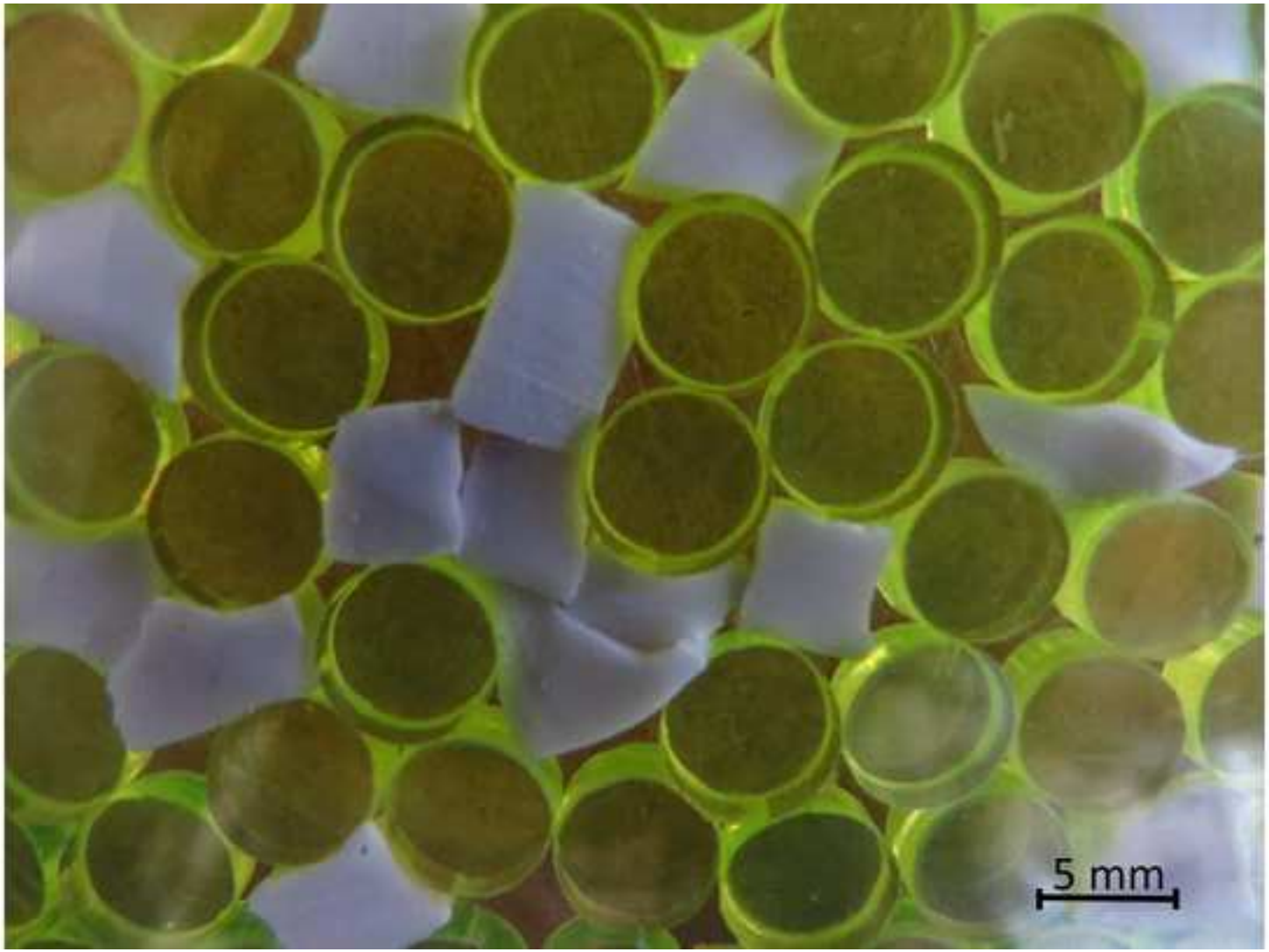

Figure 2a

Click here to access/download;Figure;Fig2a.tif

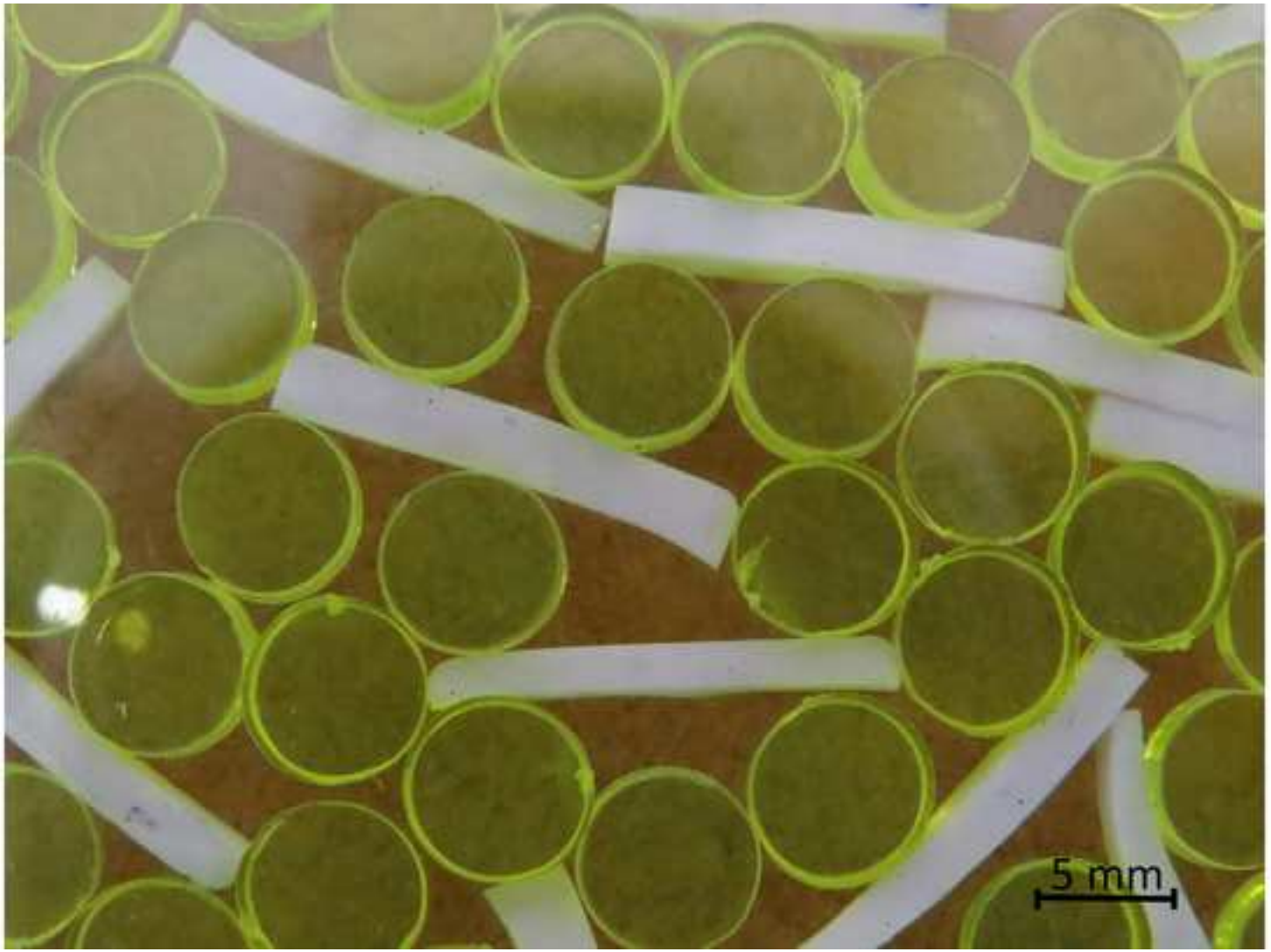

Figure 2b

Click here to access/download;Figure;Fig2b.tif

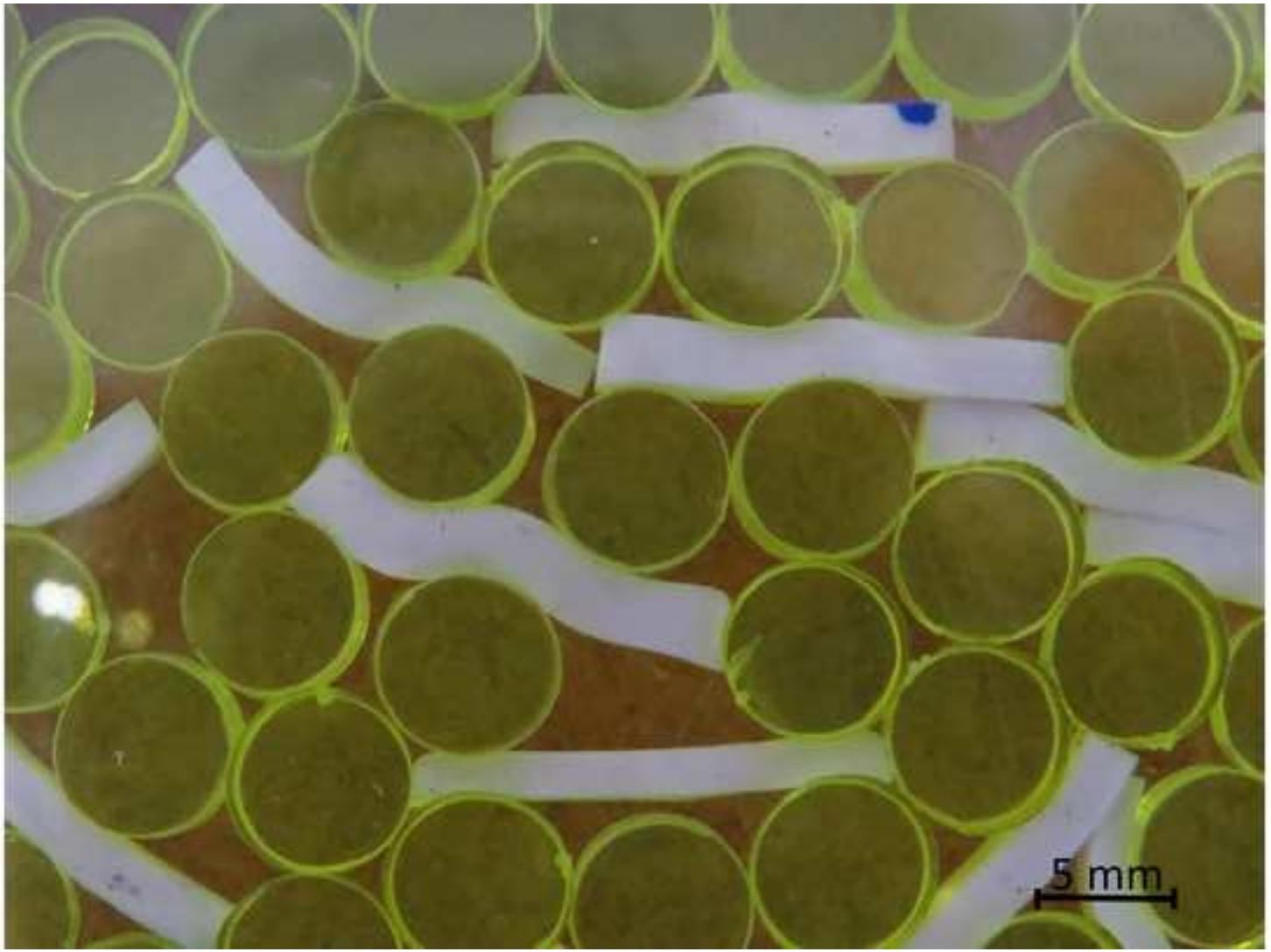

Figure 3

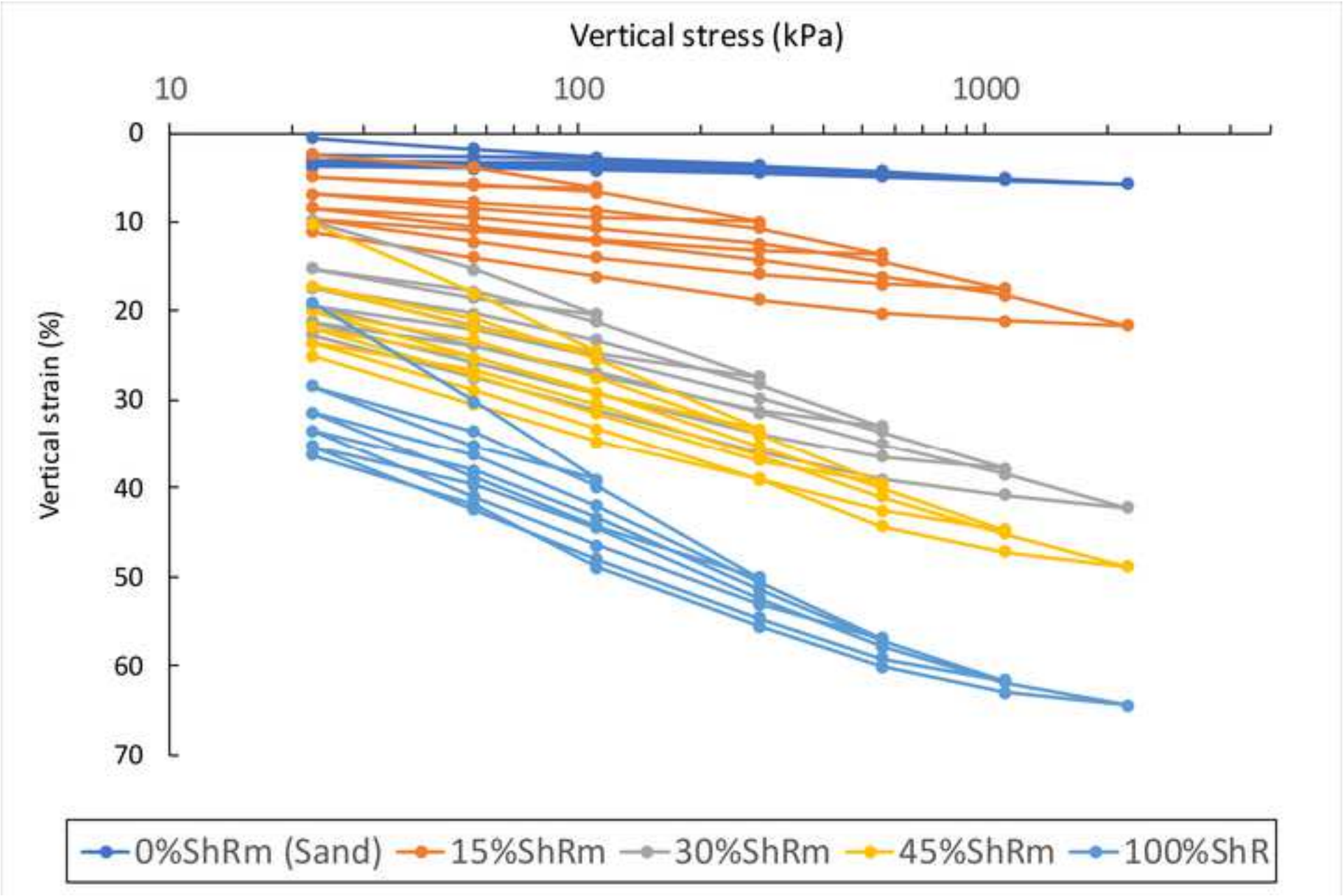

Figure 4a

Click here to access/download;Figure;Fig4a.tif

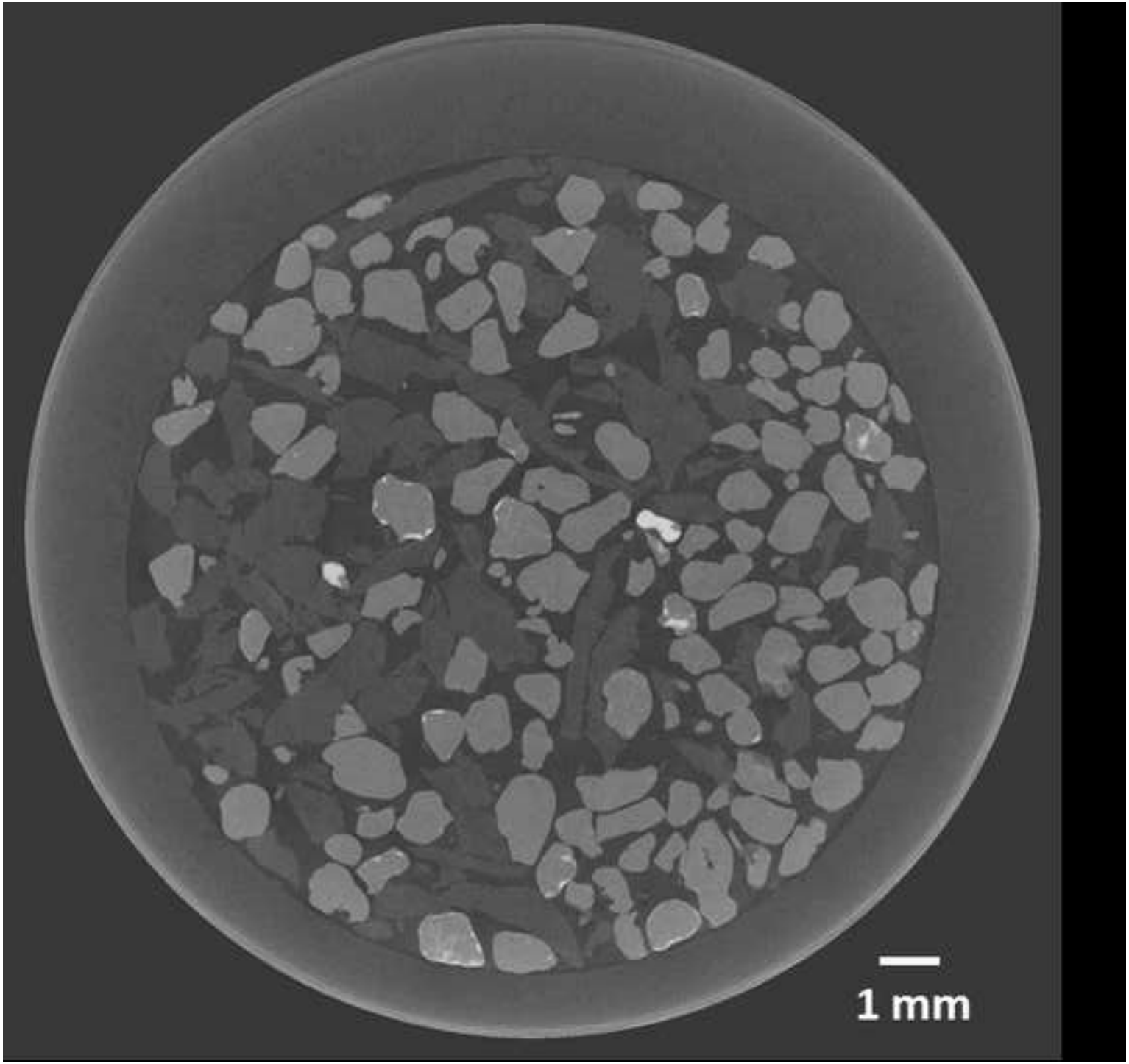

Figure 4b

Click here to access/download;Figure;Fig4b.tif

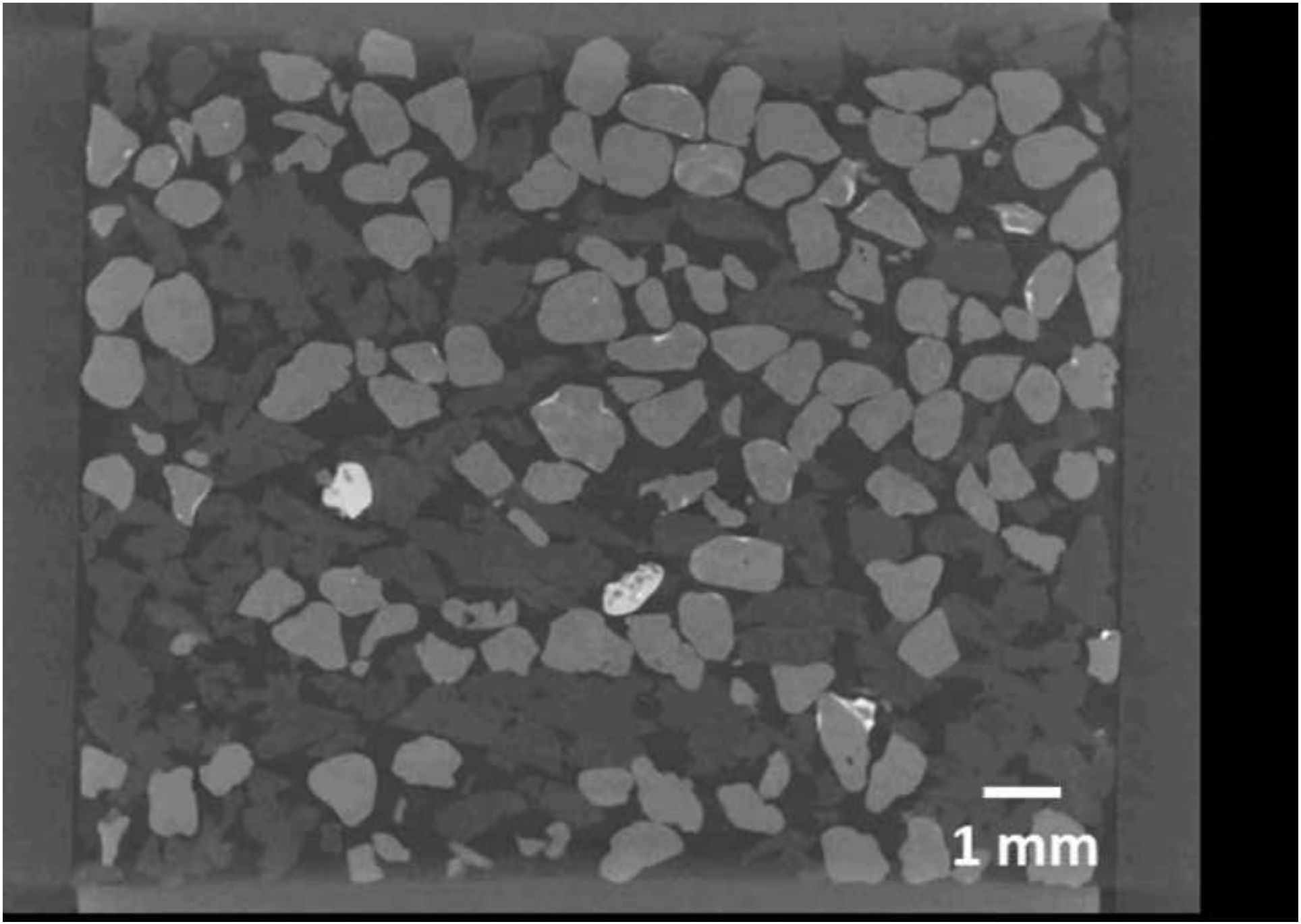

Figure 5a

Click here to access/download;Figure;Fig5a.tif

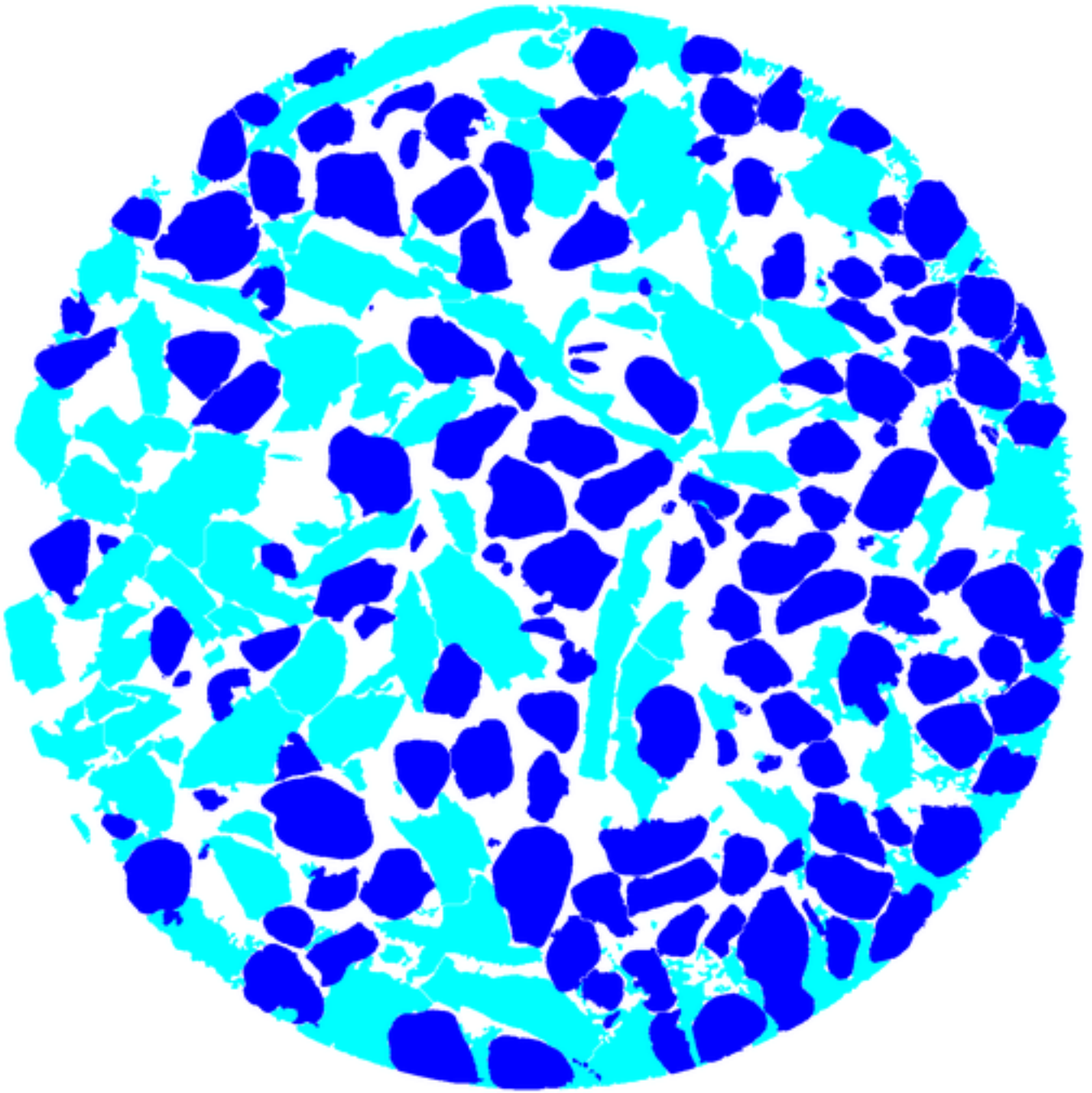

Figure 5b

Click here to access/download;Figure;Fig5b.tif

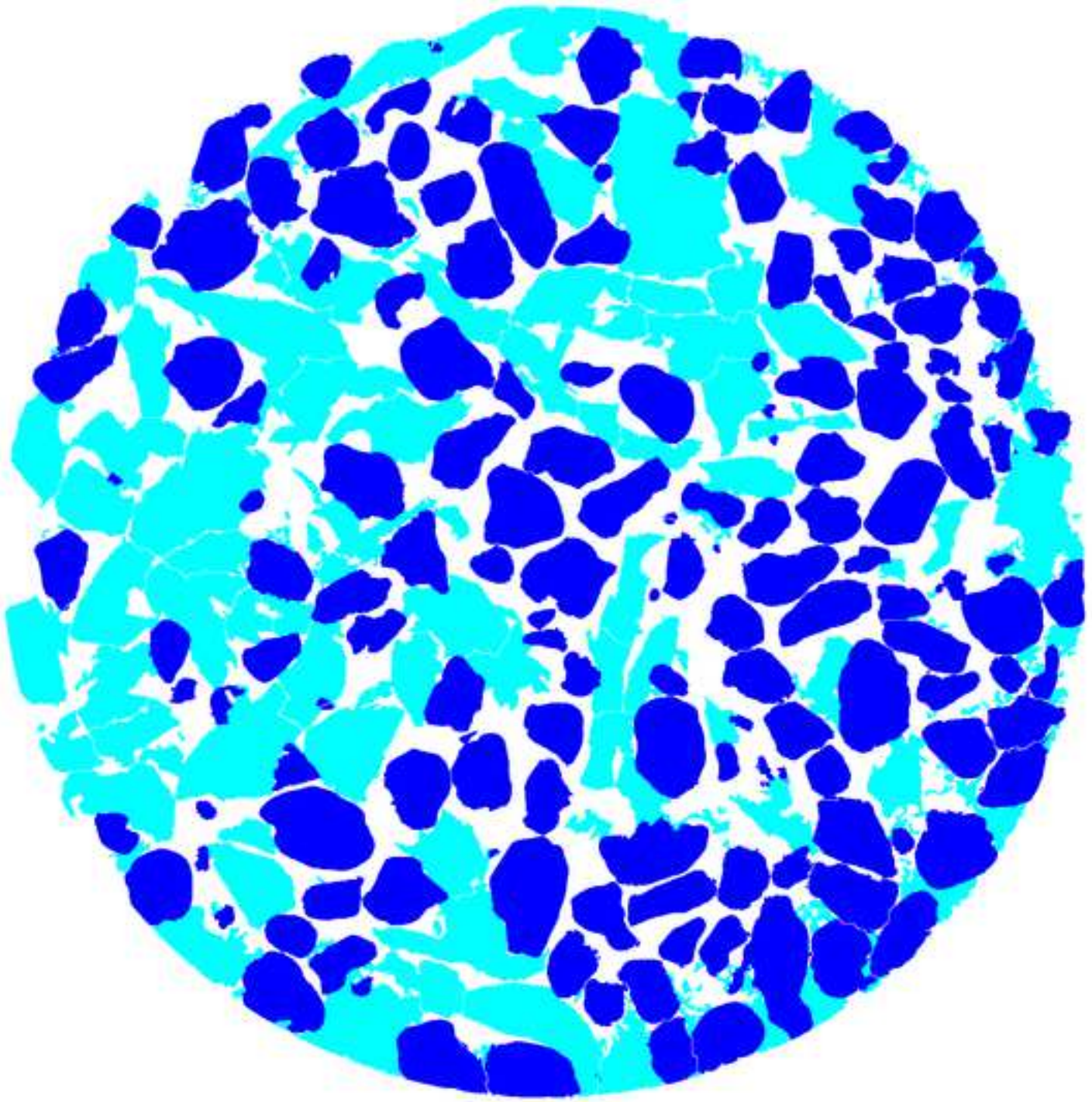

Figure 5c

Click here to access/download;Figure;Fig5c.tif

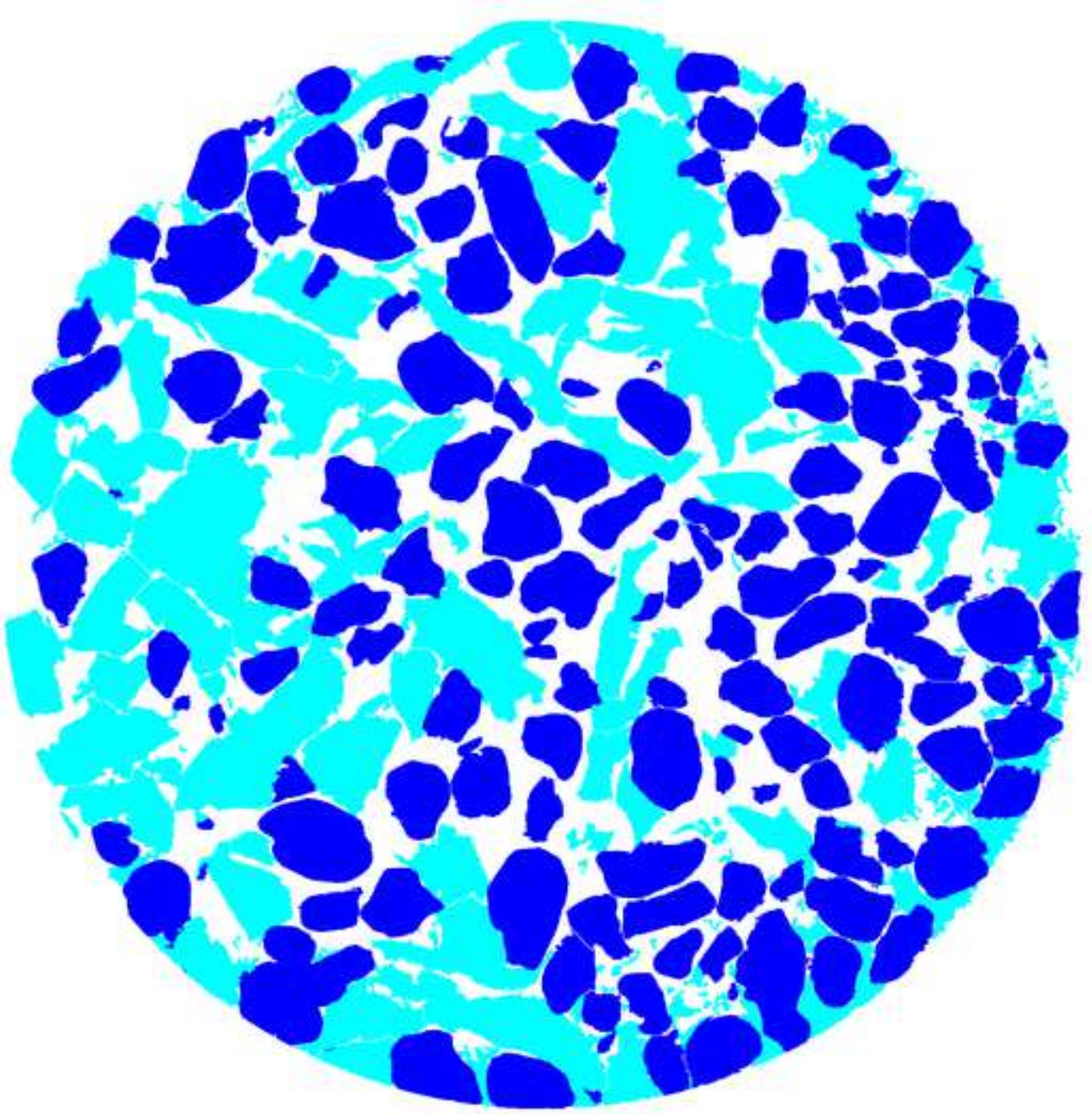

Figure 5d

Click here to access/download;Figure;Fig5d.tif

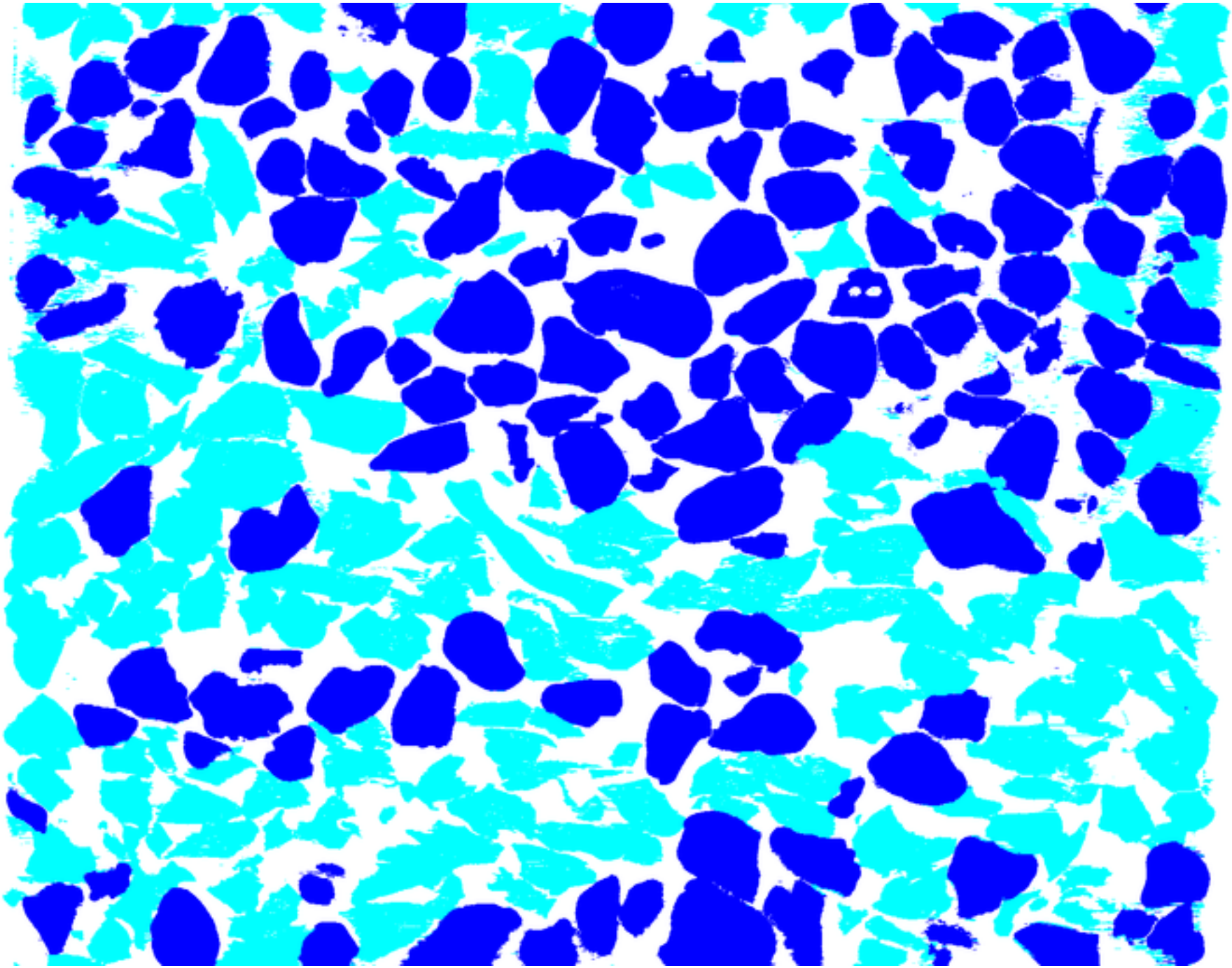

Figure 5e

Click here to access/download;Figure;Fig5e.tif

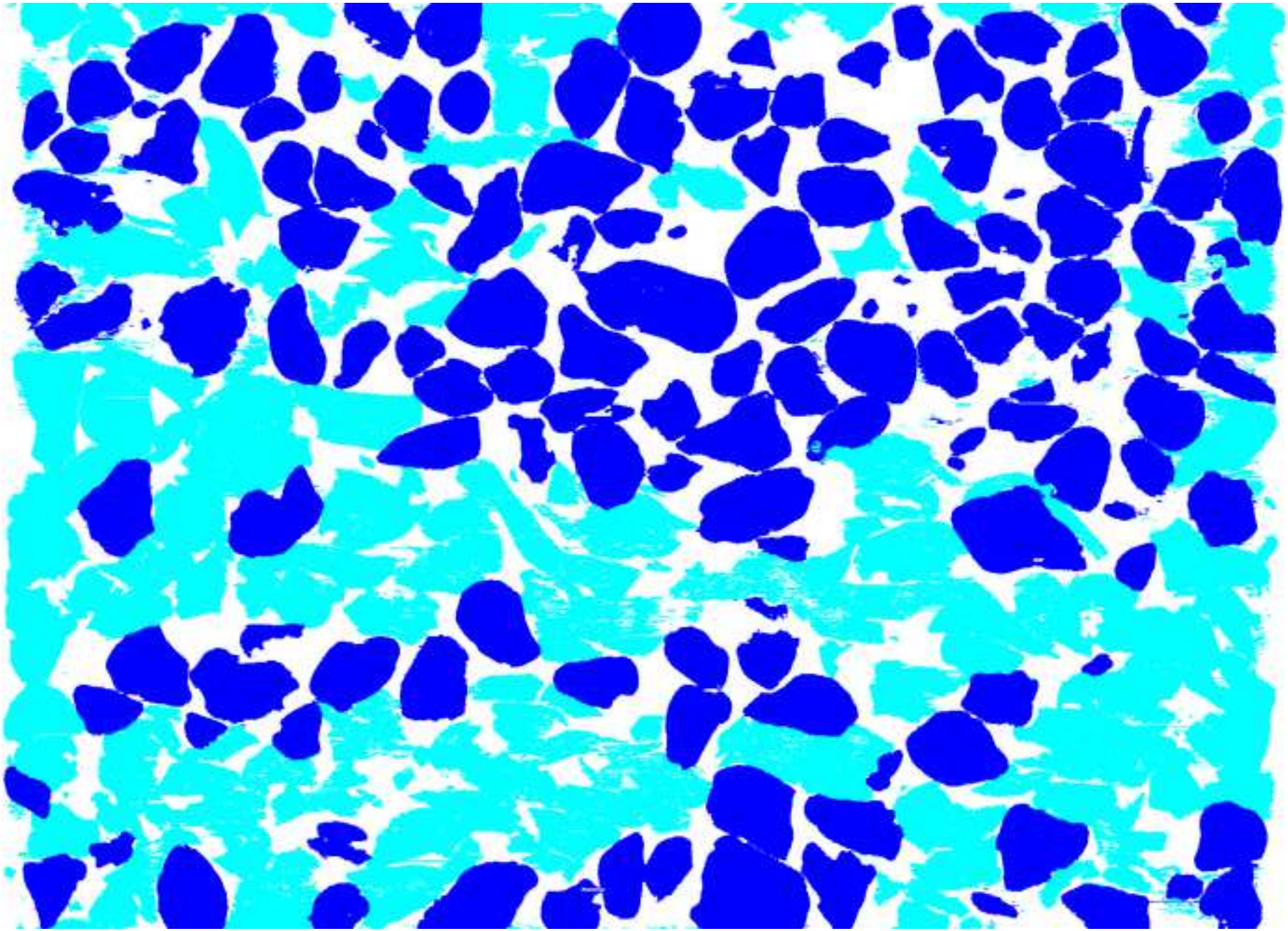

Figure 5f

Click here to access/download;Figure;Fig5f.tif

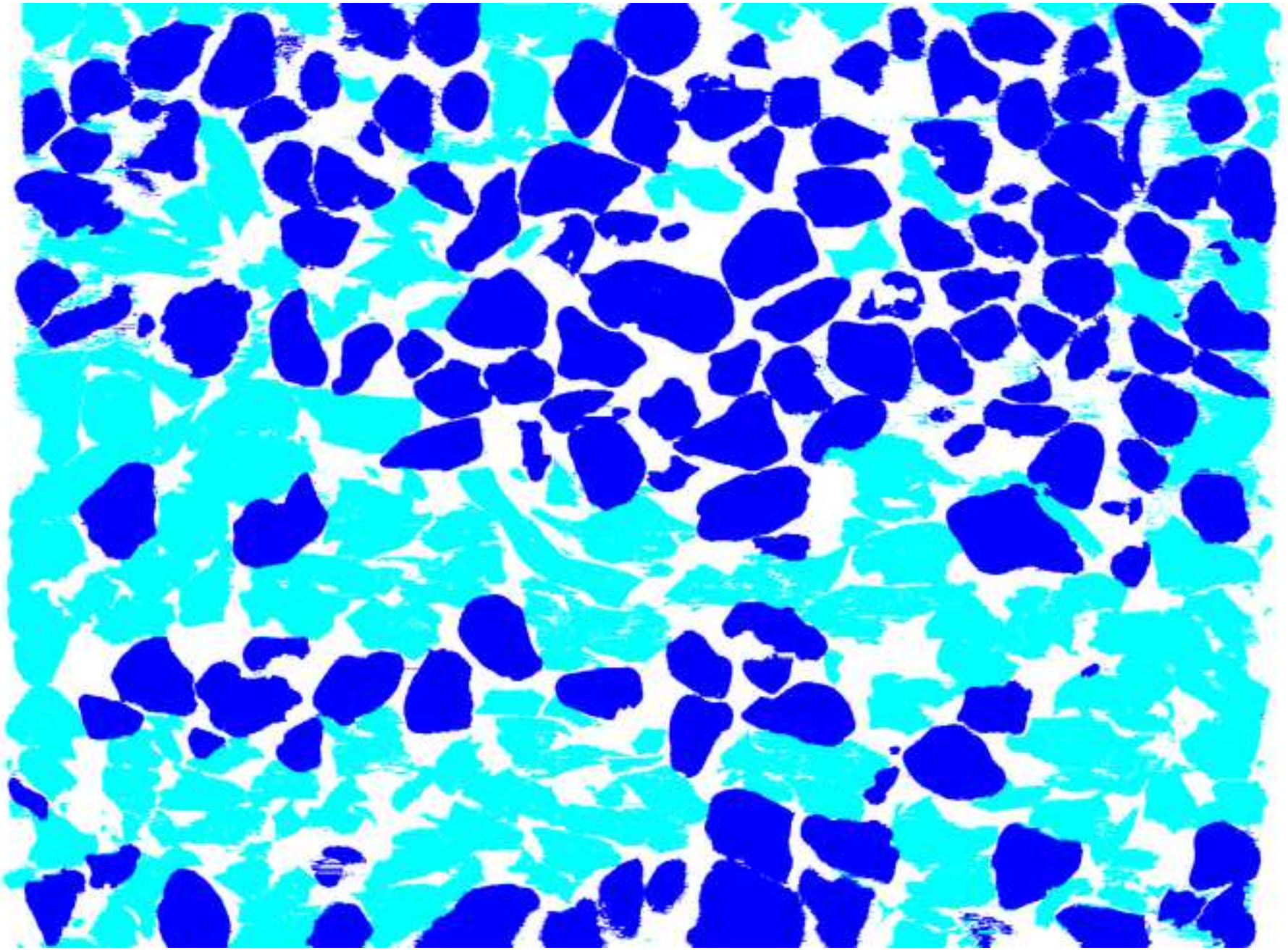

Figure 6

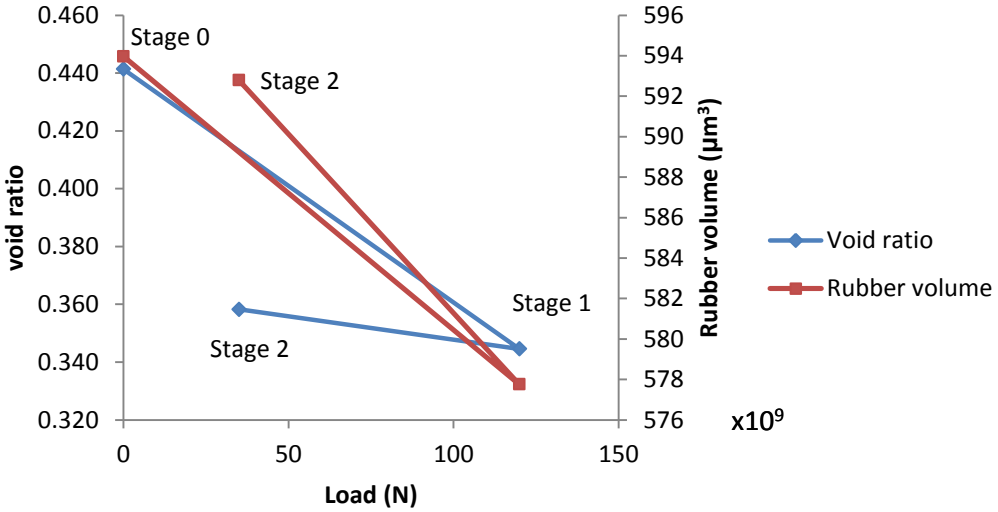

Figure 7

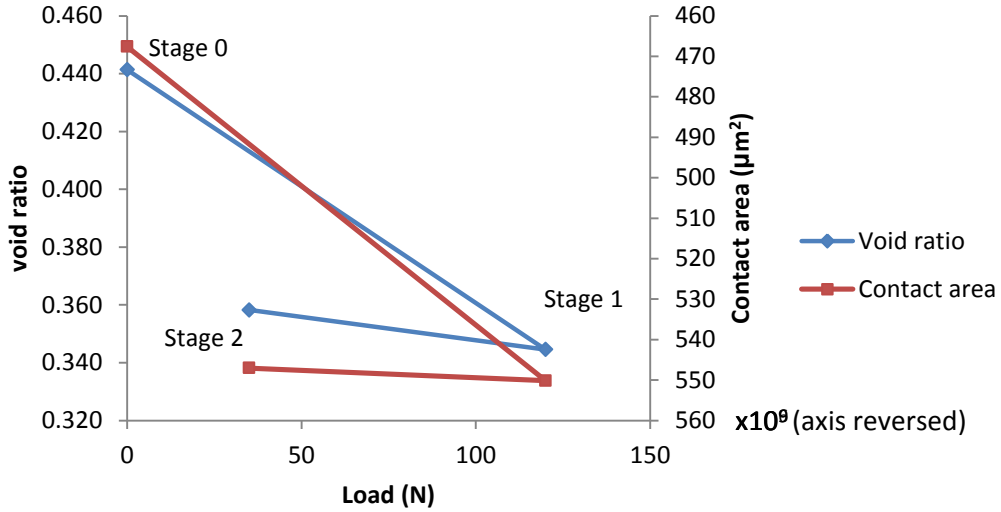

Copyright form